Biochemistry

 Volume 38, Number 27 July 6, 1999

Accelerated Publications

Potassium and Sodium Binding to the Outer Mouth of the K^+ Channel†

Leonardo Guidoni,‡ Vincent Torre,‡ and Paolo Carloni*,‡,§

Scuola Internazionale Superiore di Studi Avanzati and Istituto Nazionale di Fisica della Materia, Via Beirut 2-4, 34014, Trieste, Italy, and International Center for Genetic Engineering and Biotechnology, AREA Science Park, Padriciano 99, 34012, Trieste, Italy

Received March 8, 1999; Revised Manuscript Received May 11, 1999

ABSTRACT: Molecular dynamics simulations of the K^+ channel from *Streptomyces lividans* (KcsA channel) were performed in a membrane-mimetic environment with Na^+ and K^+ in different initial locations. The structure of the channel remained stable and well preserved for simulations lasting up to 1.5 ns. Salt bridges between Asp80 and Arg89 of neighboring subunits, not detected in the X-ray structure, enhanced the stability of the tetrameric structure. Na^+ or K^+ ions located in the channel vestibule lost part of their hydration shell and diffused into the channel inner pore in less than a few hundred picoseconds. This powerful catalytic action was caused by strong electrostatic interactions with Asp80 and Glu71. The hydration state of the metal ions turned out to depend significantly on the conformational flexibility of the channel. Furthermore, Na^+ entered the channel inner pore bound to more water molecules than K^+. The different hydration state of the two ions may be a determinant factor in the ion selectivity of the channel.

The recent determination of the crystal structure of the K^+ channel from *Streptomyces lividans* (*1*) opens a new avenue in understanding the energetics of fundamental processes such as permeation, ion binding, and selectivity. Molecular dynamics (MD)[1] simulations based on this structure allow for an accurate calculation of thermodynamic quantities necessary to understand the structural and functional role of key amino acids (*2*−*7*). Furthermore, the theoretical framework based on MD simulations will help to understand the electrophysiological experiments performed on wild-type and mutant channels.

The KcsA channel is formed by four identical subunits. Each subunit is composed of 158 residues, 97 of which could be detected in the crystallographic structure (*1*). Three binding sites of the potassium atoms have been identified, in agreement with the traditional view that K^+ channels are multiion channels (*8*−*10*). The selectivity filter, located between the first and second binding site, is a narrow funnel with a diameter of 3 Å, lined with backbone carbonylic oxygen atoms (*11*). The KcsA channel is selective for K^+ over Na^+, similarly to usual K^+ channels.[2] In this report we describe MD simulations performed with a KcsA channel embedded in a layer of *n*-octane separating two water phases.

† This work was supported by a Biotechnology grant from the EC (No. 960593) and by the Ministero dell' Università e della Ricerca Scientifica e Tecnologica (M.U.R.S.T.-COFIN).

* To whom correspondence should be addressed. E-mail: carloni@sissa.it.

‡ Scuola Internazionale Superiore di Studi Avanzati and Istituto Nazionale di Fisica della Materia.

§ International Center for Genetic Engineering and Biotechnology.

[1] Abbreviations: KcsA channel, K^+ channel from *Streptomyces lividans*; MD, molecular dynamics; OPLS, optimized potential for liquid simulations.

[2] The selectivity ratio between Na^+ and K^+ P_{Na^+}/P_{K^+} based on the reversal potential in biionic conditions is less than 0.07 in potassium channels (*12*). This ratio in the KcsA channel is 0.35 (*13*). See also ref *14*.

10.1021/bi990540c CCC: $18.00
Published on Web 06/15/1999

COMPUTATIONAL SECTION

Protein Model. Our modeling is based on the structure of the KcsA potassium channel from *S. lividans* solved at 3.2 Å resolution (*1*) [Protein Data Bank (*15, 16*) accession number 1BL8]. Part of the side chains of five amino acids (Arg27, Ile60, Arg64, Glu71, Arg117) missing in the X-ray structure were added, taking care to avoid nonphysical contacts with the rest of the protein; in particular, the missing atoms of the Glu71 side chains were added so as to point toward the NH groups of the Tyr78 backbone (see Figure 3B) (*17*). The only histidine present in the protein (His25) was assumed to be protonated in the N_δ position, as the latter forms an H-bond to the carbonyl group of Ala109. The cytoplasm/membrane environment was mimicked by a water/*n*-octane bilayer enclosed in a box of approximately 69 × 65 × 66 Å^3. This approach supplies a stable hydrophilic/hydrophobic liquid interface quickly adaptable to the protein structure and has been already successfully reported in the literature (*18, 19*). The portion of the protein immersed in the organic liquid is comprised between two layers of aromatic residues, 34 Å from each other, believed to point toward the two putative membrane/water interfaces (*1*). At physiological pH, we can assume that there are 20 positively charged Arg residues and 16 negatively charged residues (12 Glu and 4 Asp). The overall charge of the protein (+4) was neutralized by leaving the C-terminal tail of each chain deprotonated and the N-terminal tail uncharged. In the protein−K^+ and −Na^+ adducts (see below), Cl^- counterions were added close to Arg117 to balance the positive charges of the metal ions. The final systems were electroneutral, as required in performing the Ewald summation correctly (see below). The total number of atoms in our model is ∼30 000.

Parametrization. Simulations at room temperature (298 K) were carried out with the AMBER 5 package (*20*). The all-atom AMBER force field (*21*) was used for the protein. For the K^+ or Na^+ ions, the force field parameters derived by Aqvist (*22*) and adapted to the AMBER force field were used. The OPLS (*23, 24*) and the TIP3P (*25*) force fields were used for *n*-octane and water, respectively.

Molecular Dynamics Calculations. Periodic boundary conditions were applied. Electrostatic interactions were calculated with the Ewald particle mesh method (*26*) and by assuming the dielectric constant equal to 1. Bonds were constrained with the SHAKE (*27*) algorithm during the dynamics. The time integration step was set equal to 1 fs. The system was coupled to a Berendsen bath (*28*) with 0.2 ps relaxation time. The solvent was equilibrated by undergoing 0.6 ns of MD at room temperature. No phase mixing was observed. After the solute was immersed, the solvent structure underwent another 0.2 ns of MD. The entire system underwent energy minimization. Finally, several MD simulations of the protein, its R89C mutant, and complex with K^+ and Na^+ ions were performed with the following: (i) the K^+−protein complex (K^+ located in the first binding site); (ii) K^+ (or Na^+) located in the external mouth (the position was first constrained at 6 Å from the binding site in the extracellular direction during thermalization); (iii) same as (ii) but without constraint; (iv) same as (iii) with another K^+ ion located inside the pore (here the last snapshot of simulation i was taken as the initial structural model); (v) the K^+−R89C mutant complex (K^+ located in the first binding site). The calculated simulation times were (i) 1.5 ns, (ii−iv) 0.3 ns, and (v) 0.7 ns. The first 0.12 ns were used for heating the systems from 0 to 298 K. All the structural models exhibited a good Ramachandran plot with no residues in outlying regions.

All the MD calculations were carried out with the SANDER module of the AMBER 5 suite of programs (*20*) running on a four-processor SGI Origin 200 parallel machine at 0.6 h/ps. Molecular structures were drawn using Cerius[2] (*29*) and VMD (*30*).

RESULTS AND DISCUSSION

During the dynamics, the structure of the channel−K^+ complex (Figure 1A) was stable; after 0.5 ns, and for the rest of the simulation (up to 1.5 ns), atoms of the protein backbone fluctuated with a root-mean-square (rms) displacement with respect to the starting structure of 2.3 ± 0.1 Å. Residues forming the turret (from 52 to 61) experienced larger fluctuations (4.0 ± 1.2 Å) than those lining the selectivity filter (residues 75−79) (1.5 ± 0.3 Å), as shown in Figure 1B. The relatively high stability of the selectivity filter may be an important physical mechanism for ionic selectivity (*31*). The quaternary structure of the channel was stabilized by the formation of salt bridges between the Arg89 and Asp80 in neighboring subunits (Figure 1C), not evident in the X-ray structure. Some of these salt bridges broke and formed on the nanosecond time scale (Figure 1D). Force field based calculations (*20*−*25*) show that these salt bridges are very important for the integrity of the quaternary structure as they account for approximately half of the total subunit−subunit association energy. The proposed role of these two residues agrees with the observation of structural similarity between the KcsA channel and eukaryotic K^+ channels (*32*) and with conservation of these residues in a variety of K^+ channels.[3] To further explore the Asp80−Arg89-induced subunit−subunit stabilization, a simulation where Arg89 was mutated into a cysteine (R89C mutant) was performed. The calculation mimicked the experiment of Perozo et al. (*33*), which showed that this mutation essentially abolishes protein expression in the KcsA channel. Analogous mutations in other K^+ channels revealed a similar loss of functional expression: D378T and D378C in Kv2.1 (*34, 35*) and K456D in Shaker (*36*). After a few hundred picoseconds, the quaternary structure of the mutant lost its original conformation (Figure 2) and the selectivity filter became wider (Figure 2B). Our calculations therefore suggest that the loss of the functional expression of K^+ channels where the aspartate and/or the arginine (or lysine) residues near the external vestibule were mutated (*33*−*36*) was due to a partial disruption of the quaternary structure and of the selectivity filter. A simulation in the absence of K^+ ion in the binding site also indicated the important role of the metal ion in

[3] Asp80 and Arg89 (or Lys89) are conserved in the pore region of K^+ channels from several organisms (*1*): KcsA, *Streptomyces lividans* (PIR S60172); *Escherichia coli* (GenBank U24203); *Clostridium acetobutylicum* (Genome Therapeutics Corp.); *Paramecium tetraaurelia* (GenBank U19908); *Caenorhabditis elegans* (GenBank AF005246); *Mus musculus* (PIR A48206); Shaker, *Drosophila melanogaster* (PIR S00479); *Homo sapiens* (Swissprot Q09470); *Homo sapiens* (PIR S31761); *Homo sapiens* (GenBank AF031815). A more complete alignment has been done by Shealy et al. (*43*).

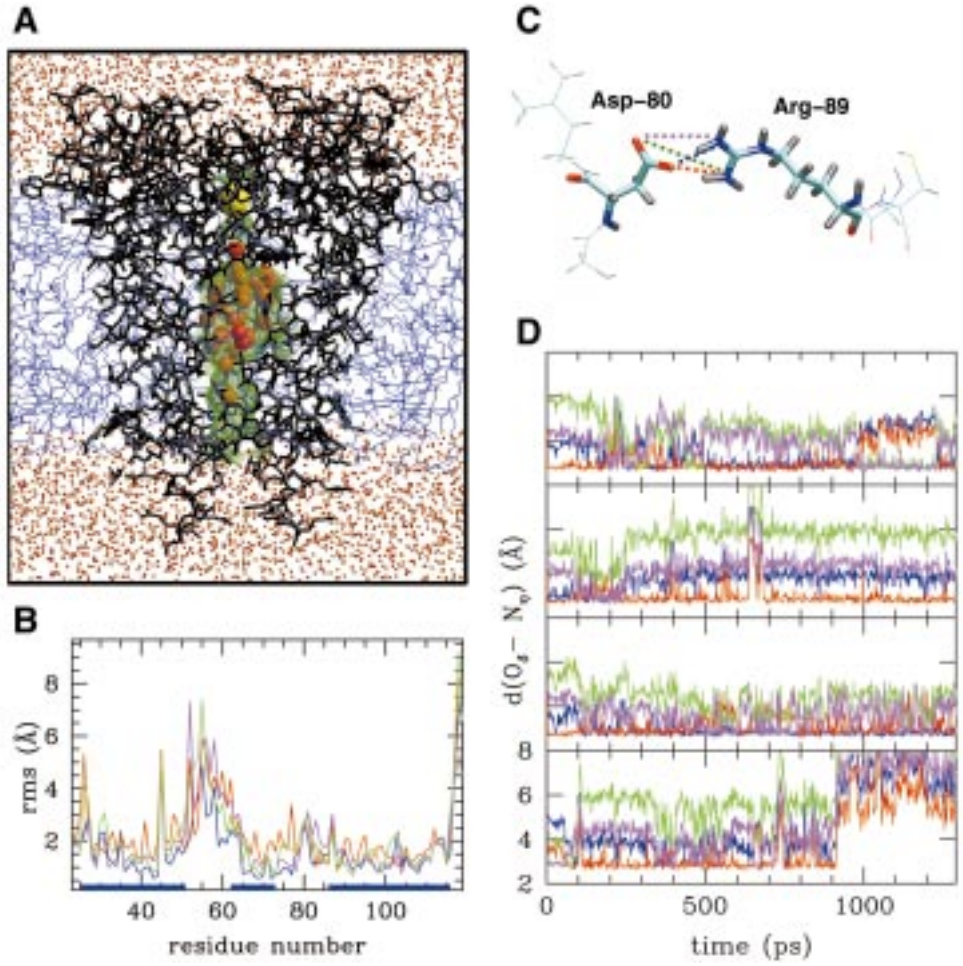

FIGURE 1: Molecular dynamics of the protein−K^+ complex. (A) The protein is immersed in an octane−water bilayer (blue and red, respectively) with a potassium ion (in yellow). The Connolly surface (*41*) within the channel pore is in green. (B) rms fluctuations per residue from the protein starting structure. The four colors (magenta, green, red, and blue) refer to the four subunits, while the blue bars on the abscissas indicate the inner (residues 25−51), the pore (residues 62−73), and the outer (residues 86−116) helices. (C) View of the Asp80−Arg89 salt bridge and (D) corresponding carboxylate oxygen−guanidinium nitrogen distances plotted as a function of time. Distances are plotted for the four Asp80−Arg89 pairs.

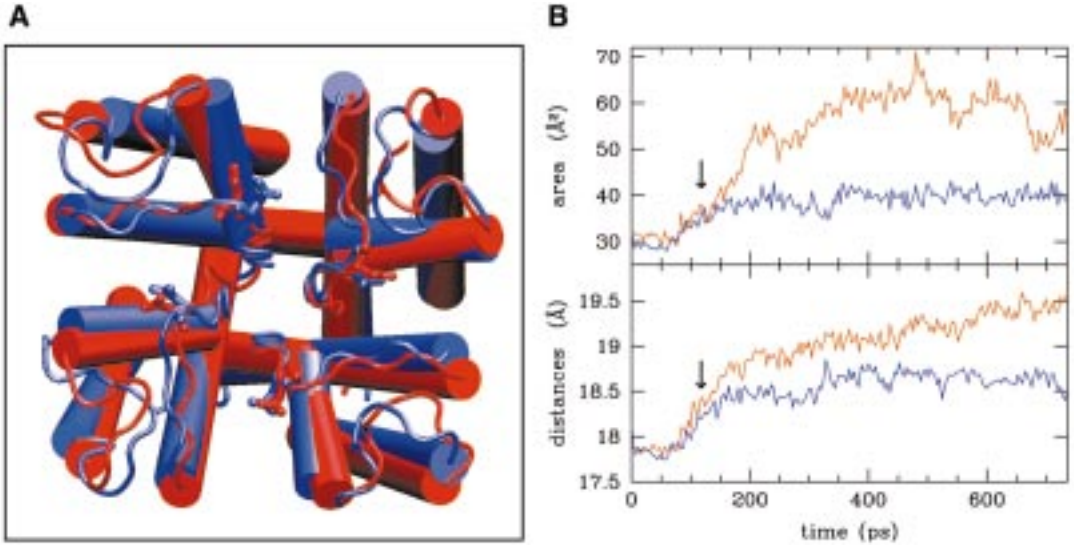

FIGURE 2: Molecular dynamics of the KcsA (blue) and its R89C mutant (red). (A) Comparison between the two structures after 450 ps (α-helices indicated as cylinders). (B) Selected geometrical features as a function of time. Bottom: average distances between the center of mass of the four subunits. Top: pore area of the four subunit pore walls (from residues from 76 to 79). The mutant channel exhibits a larger drift than the wild-type KcsA channel. The arrow indicates the time when thermalization at 298 K was achieved.

protein stability. Indeed, the selectivity filter region backbone (Tyr75−Gly79) of the KcsA channel, without a K^+ inside, experienced larger mobility than that of the KcsA channel with a K^+ ion in the inner pore (rms fluctuations were 1.9

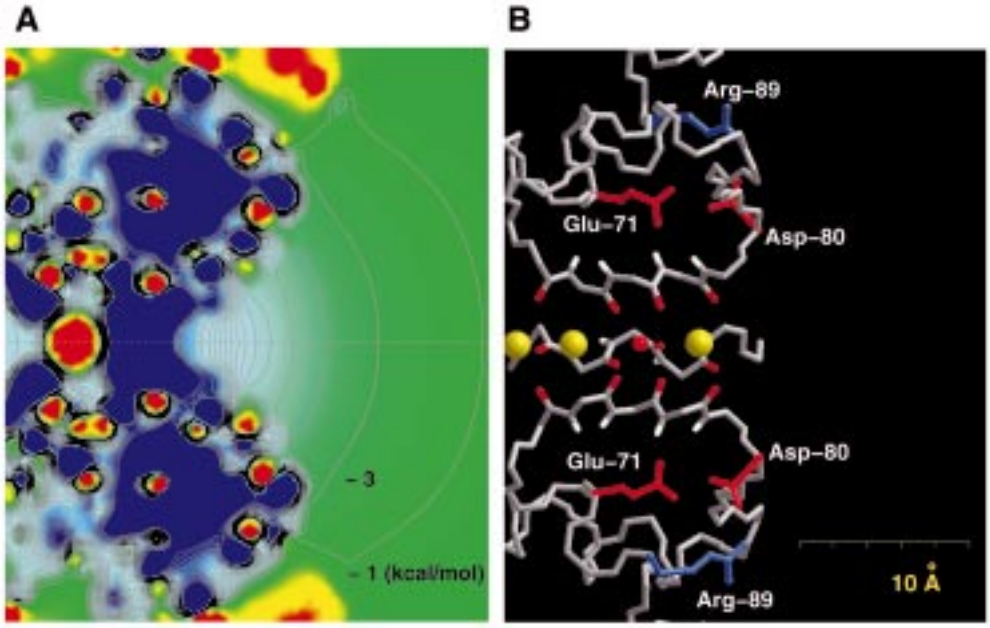

FIGURE 3: Electrostatic energy profile in the outer mouth of the KcsA channel. (A) Electrostatic potential energy (*37*, *38*) in the pore and solvent regions through a planar section containing the channel axis. The initial configuration of the KcsA channel was used with a potassium ion in the second binding site. Black lines indicate isoenergy contours at a 2 kcal/mol separation. Red (blue) indicates a very positive (negative) electrostatic energy and therefore cation repulsion (attraction). (B) Structure of some residues contributing to the electrostatic energy profile in A. The three yellow spheres indicate the three binding sites. The first binding is the more external. The small red sphere is the oxygen of the crystallographic water molecule. Also shown are backbone oxygens (red) and the amide hydrogens (white) in the selectivity filter of three subunits and Asp80 and Glu71 of two opposing subunits (red) and two Arg89 of the two other subunits (blue). Diagrams in (A) and (B) are on the same scale.

$\pm$ 0.5 and 1.0 $\pm$ 0.3 Å, respectively).

The electrostatic potential energy of the protein [calculated with the Poisson−Boltzmann equation (*37*, *38*)][4] was significantly negative in the channel vestibule and close to the first binding site (Figure 3A). The energy profile turned out to be very similar in the presence or absence of a K^+ ion in the second binding site. Thus the KcsA channel attracts cations and repels anions from its inner pore. Our electrostatic energy analysis (*20*−*25*, *37*, *38*) also showed that this valence selectivity was largely caused by the external ring of Asp80 and the inner ring of Glu71 (Figure 3B). The ring of positively charged Arg89 (Figure 3B), located more distant from the channel axis, reduced but not abolished the attraction of cations. When a potassium ion was in the first binding site, the electrostatic potential energy in the channel vestibule was less negative.

The metal binding to the protein was studied by locating hydrated K^+ or Na^+ ions in the outer vestibule. Simulations carried out with, and without, potassium in the second binding site led to similar results. At the beginning of the simulations ions were located in the bulk solvent (at 6 Å from the pore region) and were coordinated by six (Na^+) or eight (K^+) water molecules (first panels of Figure 4A,C). Both ions diffused within a few tens of picoseconds toward the first binding site (second panels of Figure 4A,C) and lost part of their hydration shell (Figure 4B,D). Diffusion occurred in the absence of any external driving force. K^+ was coordinated to two water molecules and to the backbone carbonylic oxygen atoms of Gly77 and Val76 (last panel of Figure 4A). Na^+ was coordinated to three water molecules and to the backbone oxygen atoms of Gly77 and Tyr78 (last panel of Figure 4C). Thus potassium was coordinated to less water molecules than sodium and entered deeper into the channel inner pore. As the selectivity filter has larger fluctuations in the absence of K^+ in its inner pore, the exact number of water molecules coordinated to the ions depended on the time during which the inner pore remained empty (but on average more water molecules remained bound to Na^+ than to K^+). The different hydration state of Na^+ and K^+ in the channel inner pore seems to be a basic factor determining ionic selectivity (*31*).

From these simulations several conclusions can be drawn on both structural and functional aspects of ion permeation through the KcsA channel. First, the channel is engineered so as to repel anions and attract cations, i.e., K^+ and Na^+, into the first binding site within the pore (Figure 3A). This valence selectivity in an electrically neutral channel is achieved by the specific channel conformation, with negative charges located near to the channel axis (Figure 3B). Second, when the channel is not yet occupied by a cation, the charge configuration of the KcsA channel is able to strip most of water molecules from a hydrated cation (Figure 4), thus efficiently catalyzing dehydration. As a consequence, the rate-limiting process requiring thermal activation is the removal of the permeating cation from the binding sites. The calculated time scale of the dehydration process of K^+ (a few tens of picoseconds) is fully consistent with available experimental data: indeed, quasi-elastic neutron scattering measurements (*39*, *40*) established that the residence time of water molecules bound to K^+ in aqueous solution is not greater than 100 ps. Third, a major difference between Na^+ and K^+ in the channel pore is that Na^+ keeps more water molecules attached than K^+. Finally, these simulations reveal

[4] Dielectric constants $\epsilon = 78$ and $\epsilon = 2$ were used for water and for the protein, respectively.

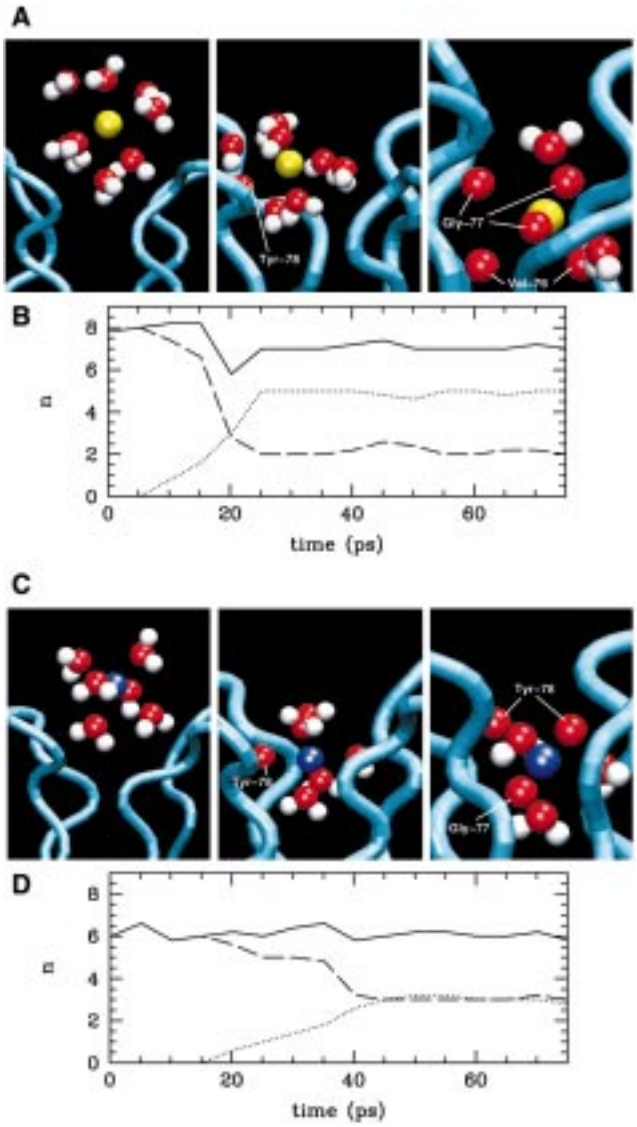

FIGURE 4: Binding of Na^+ and K^+ to the channel. Top: selected snapshots [(A) after 2 (left), 16 (middle), and 60 (right) ps; (C), after 2 (left), 24 (middle), and 60 (right) ps] are shown for both K^+ (A) and Na^+ (C) cations; ions are completely hydrated in the outer mouth of the vestibule (left), interact with the protein (middle), and diffuse into the first binding site (right). Coordination numbers (n) of K^+ (B) and Na^+ (D) plotted as a function of time. n is calculated assuming a K^+− (Na^+−) ligand cutoff of 3.65 (3.25) Å (*42*). Total coordination numbers (solid line) and contributions from the solvent (dashed) and from the backbone (dotted line) are reported.

a novel role for Asp80, usually thought to be an external binding site, forming salt bridges with Arg89 and therefore contributing to the stability of the tetrameric complex.

ACKNOWLEDGMENT

We thank R. MacKinnon for providing us with the coordinates of the KcsA channel; F. Alber for running the DELPHI program; A. Laio for helpful discussion; and S. Baccaro, L. De Santis, and G. Settanni for comments on the manuscript.

REFERENCES

1. Doyle, D. A., Cabral, J. M., Pfuetzner, R. A., Kuo, A., Gulbis, J. M., Cohen, S. L., Chait, B. T., and MacKinnon, R. (1998) *Science 280*, 69−77.
2. Roux, B., and Karplus, M. (1994) *Annu. Rev. Biophys. Biomol. Struct. 23*, 731.
3. Tieleman, D. P., and Berendsen, H. J. C. (1998) *Biophys. J. 74*, 2786−2801.
4. Sansom, M. S. P. (1998) *Curr. Opin. Struct. Biol. 8*, 237−244.
5. Kollman, P. A., and Merz, K. M. (1990) *Acc. Chem. Res. 23*, 246.
6. van Gunsteren, W. F. (1989) *Computer Simulation of Biomolecular Systems*, ESCOM Science Publishers, Leiden.
7. Zhong, Q., Husslein, T., Moore, P. B., Newns, D. M., Pattnaik, P., and Klein, M. L. (1998) *FEBS Lett. 434*, 265−271.
8. Hodgkin, A. L., and Keynes, R. D. (1955) *J. Physiol. 128*, 61−88.
9. Hille, B., and Schwartz, W. J. (1978) *Gen. Physiol. 72*, 409−442.
10. Hagiwara, S., and Takahashi, K. (1974) *J. Membr. Biol. 18*, 61−80.
11. Armstrong, C. (1998) *Science 280*, 56−57.
12. Hille, B. (1992) *Ionic Channels of Excitable Membranes*, Sinauer Associates, Sunderland, MA.
13. Schrempf, H., Schmidt, O., Kummerlen, R., Hinnah, S., Muller, D., Betzler, M., Steinkamp, T, and Wagner, R. (1995) *EMBO J. 14*, 5170−5178.
14. Cuello, L. G., Romero, J. G., Cortes, D. M., and Perozo, E. (1998) *Biochemistry 37*, 3229−3236.
15. Sussman, J. L., Lin, D., Jiang, J., Manning, N. O., Prilusky, J., Ritter, O., and Abola, E. E. (1998) *Acta Crystallogr. D54*, 1078−1084.
16. Abola, E. E., Sussman, J. L., Prilusky, J., and Manning, N. O. (1997) *Methods Enzymol. 277*, 556−571.
17. Gouaux, E. (1998) *Structure 15*, 1221−1226.
18. Zhong, Q., Jiang, Q., Moore, P. B., Newns, D. M., and Klein, M. L. (1988) *Biophys. J. 74*, 3−10.
19. Moore, P. B., Zhong, Q., Husslein, T., and Klein, M. L. (1998) *FEBS Lett. 431*, 265−271.
20. Case, D. A., Pearlman, D. A., Caldwell, J. W., Cheatham, T. E., III, Ross, W. S., Simmerling, C. L., Darden, T. A., Merz, K. M., Jr., Stanton, R. V., Cheng, A. L., Vincent, J. J., Crowley, M., Ferguson, D. M., Radmer, R. J., Seibel, G. L., Singh, U. C., Weiner, P. K., and Kollman, P. A. (1997) *AMBER 5*, University of California, San Francisco.
21. Cornell, W. D., Cieplak, P., Bayly, C. I., Gould, I. R., Merz, K. M., Jr, Ferguson, D. M., Spellmeyer, D. C., Fox, T., Caldwell, J. W., and Kollman, P. A. (1995) *J. Am. Chem. Soc. 117*, 5179−5196.
22. Aqvist, J. (1990) *J. Phys. Chem. 94*, 8021−8024.
23. Kaminski, G., Duffy, E. M., Matsui, T., and Jorgensen, W. L. (1994) *J. Phys. Chem. 98*, 13077−13082.
24. Chen, B., Martin, M. G., and Siepmann, J. I. (1998) *J. Phys. Chem. B 102*, 2578−2586.
25. Jorgensen, W. L., Chandrasekhar, J., Madura, J. D., Impey, R. W., and Klein, M. L. (1983) *J. Chem. Phys. 79*, 926−935.
26. Essman, U., Perera, L., Berkowitz, M. L., Darden, T., Lee, H., and Pedersen, L. G. (1995) *J. Chem. Phys. B 103*, 8577−8593.
27. Ryckaert, J. P., Ciccotti, G., and Berendsen, H. J. C. (1977) *J. Comput. Phys. 23*, 327−341.
28. Berendsen, H. J. C., Postma, J. P. M., van Gunsteren, W. F., Di Nola, A., and Haak, J. R. (1984) *J. Chem. Phys. 81*, 3684−3690.
29. Cerius^2 (1997) Molecular Simulation Inc., Eugene, OR.
30. Humphrey, W., Dalke, A., and Shulten, K. (1996) *J. Mol. Graphics 14*, 33−38.
31. Laio, A., and Torre, V. (1999) *Biophys. J. 76*, 129−148.
32. MacKinnon, R., Cohen., S. L., Kuo, A., Lee, A., and Chait, B. T. (1998) *Science 280*, 106−109.
33. Perozo, E., Cortes, D. M., and Cuello, L. G. (1998) *Nat. Struct. Biol. 5*, 459−469.
34. Kirsch, G. E., Pascual, J. M., and Shieh, C. C. (1995) *Biophys. J. 68*, 1804−1813.
35. Pascual, J. M., Shieh, C. C., Kirsch, G. E., and Brown, A. M. (1995) *Neuron 14*, 1055−1063.
36. Goldstein, S. A. N., Pheasant, D. J. and Miller, C. (1994) *Neuron 12*, 1377−1388.

37. Honig, B., and Nicholls, A. (1995) *Science 268*, 1144−1149.
38. Gilson, M., Sharp, K., and Honig, B. (1988) *J. Comput. Chem. 9*, 327−335.
39. Ohtaki, H., and Radnai, T. (1993) *Chem. Rev. 93*, 1157−1204.
40. Friedman, H. L. (1985) *Chem. Scr. 25*, 42.
41. Connolly, M. L. (1983) *Science 221*, 709−713.
42. Song, H. L., and Jayendran, C. R. (1996) *J. Phys. Chem. 100*, 1420−1425.
43. Shealy, R., Murphy, A., Ramarathnam, R., Subramaniam, S., and Jakobsson, E. (1999) *Biophys. J. 76*, A190.

BI990540C